RSC Advances

RSC Advances

www.rsc.org/advances

ROYAL SOCIETY OF CHEMISTRY

www.rsc.org/advances

RSC Advances

PAPER

Photocatalytic Reduction of CO₂ Using Molybdenum-doped Titanate Nanotubes in MEA Solution

Hung-Yu Wu,[a] Nhat Huy Nguyen,[a] Hsunling Bai,[a]† Sue-min Chang[a] and Jeffrey C.S. Wu[b]

In this study, the photocatalytic reduction of CO_2 in monoethanolamine solution to form valuable energy sources was investigated using Mo-doped TNTs photocatalysts for the first time. The results revealed that the structure of Mo-doped TNTs was changed with the increase of calcination temperature. For Mo-doped TNTs calcined at 500 °C, the partial corruption of titanate nanotubes into anatase particles caused the reduction of Mo species from Mo^{6+} to Mo^{5+} and produced oxygen vacancies, which resulted in the highest CO_2 reduction ability. The yield rates of CH_4, CO and total combustible organic compounds were 0.52, 10.41 and 13.53 μmol/g-cat., respectively, under UVA (8W, 63μW/cm²) irradiation. The photoreduction quantum efficiencies of CH_4 and CO were achieved at 0.036% and 0.180%, respectively. It was found that the molybdenum structure and oxygen vacancies could be the key factors controlling the photocatalytic reduction efficiency of CO_2. Possible structure transformation of Mo-doped TNTs at different calcination temperatures was inferred. And reaction mechanism for photocatalytic CO_2 reduction with oxygen vacancy sites of Mo-doped TNTs was proposed.

Introduction

The rapid industrial development with increasing fossil fuel combustion is one of the major reasons which cause the continuous increase of atmospheric carbon dioxide (CO_2) level every year[1–3]. Thus reducing CO_2 emission from the fossil fuel combustion sources has become a new study field. The CO_2 capture and storage (CCS) process has been evaluated by the Inter-governmental Panel on Climate Change (IPCC) as a feasible CO_2 mitigation option[4–9]. And monoethanolamine (MEA) has been most widely employed as the absorbent for CO_2 capture[10,11].

There are many studies on direct conversion of CO_2 to other valuable energy sources, chemicals or products by solar energy. The photocatalytic reduction of CO_2 was induced with the addition of some reductants such as hydrogen[12,13], water vapor[14,15], 2-propanol[16,17], $FeCl_3$[18] and $KHCO_3$[19], etc.. As an attempt to enhance the solubility of CO_2 in water, absorbents such as KOH[19] or $NaOH$[20–22] have been added in the literature studies.

The TiO_2 photocatalyst has been extensively used in CO_2 reduction studies because of its exceptional properties such as non-toxicity and low cost. Recently, titanate nanotubes (TNTs) have attracted much attention in photocatalytic research field because their one-dimensional nanostructure have distinctive geometrical morphologies as well as physical and chemical

properties. Yu and Wang[23] indicated that titanate nanotube structure allows electrons to quickly transfer to the surface as compared to TiO_2 nanoparticles. This helps to reduce the recombination of electron-hole pairs in the process of electronic transmission. There are several methods to prepare titanate nanotubes[24–27]; nevertheless, the hydrothermal method is typically recommended for the commercial production[27,28]. In addition, the surface area and the amount of anatase phase of the TNTs can be modified by calcination at various temperatures[29–32].

The metal doping and coupling with semiconductors is a common modification method in photocatalytic studies. It was reported that among various transition metal ions, lanthanide group metals, precious metals or non-metals, e.g. copper[22], silver[33], gold[34,35], cerium[36–38], nickel[39], zinc[40], graphene[34] and nitrogen[41], in TiO_2 could advance electron–hole separation. And they were widely applied in the degradation of pollutants[34,41], water splitting[35,42] and CO_2 reduction[33,43–46]. Among many nonprecious metal-doped TiO_2 materials[22,47–49], Mo-doped TiO_2[50–52] was proven to have high potential of photocatalytic activity. However, although TNTs synthesized by hydrothermal method have many applications, to the authors' knowledge there is no literature on using Mo-TiO_2 or Mo-TNTs for the CO_2 reduction. This is because molybdenum usually exists on the TiO_2 surface as molybdenum trioxides; it could enhance oxidation ability and inhibit reduction ability of Mo-TiO_2.

In our previous study[53], MEA was used as the absorbent and Ti-MCM-41 as the photocatalyst, which can combine the CO_2 capture and utilization into a single process and produce regenerable energy by photocatalysis. However, when using Ti-MCM-41 as the photocatalyst, the CO_2 reduction could be activated only at deep UV light (254 nm). This would limit the application of this process. Besides, there is still limited

[a] Institute of Environmental Engineering, National Chiao Tung University, Hsinchu, 30010, Taiwan.
[b] Department of Chemical Engineering, National Taiwan University, Taipei, 10617, Taiwan.
† To whom correspondence should be addressed: Prof. Hsunling Bai,
Tel.: +886-3-5731868. Fax: +886-3-5725958. E-mail: hlbai@mail.nctu.edu.tw.
See DOI: 10.1039/x0xx00000x

information on the effect of chemical properties of Mo-TNTs photocatalysts and reaction mechanism in the photocatalytic reduction of CO_2 with MEA solution.

The aim of this research is thus to study the photocatalytic reduction of CO_2 in MEA solution using TNTs and Mo-doped TNTs as photocatalysts under UVA light (365nm) irradiation. The chemical reaction mechanism for CO_2 absorption and reduction ability of Mo-doped TNTs were inferred. The effect of photocatalytic properties on the CH_4 and CO yields was evaluated and the photo-reduction quantum efficiency was reported.

Experimental

Photocatalysts preparation

The TNTs were prepared by the alkaline hydrothermal method[54] while precipitation method was used for doping of Mo onto TNTs. In a typical procedure, 6 g of TiO_2 (Degussa P25) powder was mixed in 180 ml of 10 N sodium hydroxide solution for 20 min and sonicated for 20 min. The solution was then transferred into an autoclave and placed in an oven at 135 °C for 24 hrs. The resulting material was subsequently cooled and allowed to age for 12 hrs. The cooled material was washing and filtrating with 500 ml of DI water. After washing and filtrating, the material was added into 1 L of DI water. The solution was then adjusted to pH 3.0 using 0.1 N nitric acid followed by further stirring. Meanwhile, ammonium heptamolybdate $((NH_4)_6Mo_7O_{24} \bullet 4H_2O)$ with the calculated Mo/Ti molar ratio of 1% was dissolved in 40 ml of DI water, which was then added into the above solution. The resulting suspension was stirred for 30 min, and then sonicated for 30 min. After subjecting the suspension to repetitive washing with DI water, the material was dried in air at 120 °C for 12 hrs and finally calcined in air at different temperatures (120–700 °C) for 2 hrs. The materials were named as T-X or Mo-T-X, with T stands for the TNTs, X denotes the calcination temperature of the materials.

Photocatalysts characterization

The materials were characterized by different techniques for understanding their structure, absorption spectra and element types. The crystalline nature of Mo-doped TNTs was analyzed by an X-ray (wavelength λ = 1.5405 Å) diffractometer (Bruker D8 SSS) equipped with a copper target operated at 30 kV and 20 mA. The diffractograms of Mo-doped TNTs samples were recorded in the 2θ range of 10-80° with a scanning speed of 4°/min. The morphology of the materials was observed via a transmission electron microscope (TEM) (Hitachi, HT7700). An X-ray photoelectron spectroscope (XPS, ESCA PHI 1600) was used to identify the surface composition and chemical state of elements in the photocatalysts. The metal contents were determined by Inductively Coupled Plasma Atomic Emission Spectroscopy (ICP-AES) using a Jarrell-Ash ICAP9000 instrument. The specific surface area, pore volume and average pore diameter (BJH method) of the samples were measured by N_2 adsorption-desorption isotherms using a

surface area and porosity analyzer (Micromeritics, ASAP 2000). All the samples were degassed at 350 °C or lower (if their calcination temperature was lower than 350 °C) for 6 hrs under vacuum (10^{-6} mbar) prior to the adsorption experiments.

Photocatalytic reduction of CO_2

The photocatalytic activity of Mo-doped TNTs was evaluated by photocatalytic reduction of CO_2, and the experimental details can be found in our previous study[53]. In the liquid phase reaction, the catalyst loading was 0.1 g in 300 ml of 0.2M MEA solution. Before each reaction test, the solution was aerated with CO_2 (99.999%) for 1 hr to ensure the saturated absorption of CO_2. Temperature of the whole system during the experiments was controlled at 25±2°C in a temperature-controlled cabinet. Mo-doped TNTs photocatalysts were illuminated in the solution under a UVA lamp (8W, 365 nm, $63\mu W/cm^2$). The products were analyzed by a Fourier transform infrared spectroscope (FTIR, MB-104 MOMEM) and a gas chromatographer (SRI-8610C) equipped with an FID and 5 m long Porapak Q column. The major products of the reaction were expressed as total combustible organic compounds (TCOCs), which includes CH_4, CO and all other detectable organic compounds. The concentration of CH_4 and TCOCs were measured by GC-FID every hour while the concentration of CO (CH_4 and TCOCs as well) were measured by FTIR after 6 hrs tests.

Results and discussion

Catalyst characterization

To improve the CO_2 reduction ability of photocatalysts, one of the key factors is to increase the surface area of photocatalysts[55–58]. The pore characteristics of P25 (TiO_2), T-X and Mo-T-X are listed in **Table 1**. It can be observed that the pore structures of TNTs (T-X and Mo-T-X) were quite different from that of TiO_2.

Table 1. Pore characteristics of P25, pure TNTs and Mo-doped TNTs after calcination

| Catalysts		Calcination Temp.(°C)	$^aS_{BET}(m^2/g)$	$^bDP_{BJH}(nm)$	$^cV_p(cm^3/g)$
Catalyst Type	Sample Name				
TiO$_2$	P25	-	53	9.6	0.1
Pure TNTs	T-120	120	390	11.8	1.2
	T-300	300	341	13.6	1.2
	T-400	400	161	22.3	0.9
	T-500	500	106	23.5	0.6
	T-600	600	61	23.9	0.3
	T-700	700	26	54.6	0.1
Mo-doped TNTs	Mo-T-120	120	342	11.6	1.3
	Mo-T-300	300	297	12.5	1.2
	Mo-T-400	400	221	18.1	1.2
	Mo-T-500	500	110	29.7	1.1
	Mo-T-600	600	77	38.3	0.9
	Mo-T-700	700	38	36.2	0.3

NOTE: ^{a}BET surface area. ^{b}Pore volume. ^{c}Pore diameter calculated by BJH theory.

The specific surface areas of both T-X and Mo-T-X were higher than that of P25 when they were calcined at temperatures below 600 °C. For example, the specific surface areas of T-120 and Mo-T-120 were 390 and 342 m^2/g, respectively, which were 7.4 and 6.5 times higher than that of P25. Compared to the TNTs without metal doping, the doping of Mo into the TNTs led to a lower specific surface area at lower calcination temperatures (<300 °C). However, the thermal stability of Mo-doped TNTs was relatively higher as their specific surface area became larger when calcination temperature was increased to over 400°C.

When calcination temperature was further increased to 700 °C, the specific surface area and pore volume of T-700 and Mo-T-700 were significantly reduced to 26–38 m^2/g and 0.1–0.3 cm^3/g, respectively. Their pore characteristics were similar to those of P25, but the values of pore diameter were quite different which might be due to the sintering of the porous TNTs materials into large particles at high calcination temperature. **Fig. 1** shows the pore size distribution of T-Xs and Mo-T-Xs. Two obvious peaks of the pore size distribution were observed for both T-Xs and Mo-T-Xs as the calcination temperature was lower than 300–400 °C. By increasing the calcination temperatures from 400 to 700 °C, the first pore size distribution at ca. <5nm gradually disappeared.

Fig. 2 demonstrates the correlation between the specific surface area and the calcination temperature, which showed high linear correlation. The R^2 values between specific surface areas and calcination temperatures were 0.9279 and 0.9538, respectively, for T-Xs and Mo-T-Xs. These results confirmed that the specific surface areas of TNTs and Mo-doped TNTs strongly depend on the calcination temperature. **Figs. 3(A)-3(F)** display the TEM images of TNTs, Mo-doped TNTs and P25 formed after various calcination temperatures. The TNT precursor of P25 TiO$_2$ consists of large particles with sizes of 40 to 80 nm (**Fig. 3F**). After hydrothermal treatment, the as-synthesized T-120 (**Fig. 3A**) and Mo-T-120 (**Fig. 3C**) showed

nanotubular structures with diameters of 8–11 nm and lengths of a few micro-meters. After calcined at 200–700 °C for 2 hours, the morphology of TNTs and Mo-doped TNTs shifted from tubes to rods and to spherical particles. The morphology of Mo-doped TNTs at 200–300 °C still showed tubular structures but their lengths were reduced to 40 to hundreds of nanometers. There was an obvious change in morphology when the calcination temperature increased to 500 °C, at which the tubular, rod and nanoparticle structures were coexisted (**Figs. 3B and 3D**).
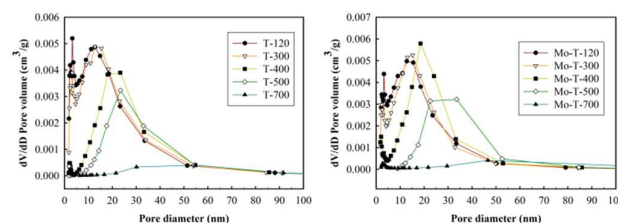
Fig. 1 The pore size distribution of TNTs and Mo-doped TNTs calcined at various calcination temperatures ranging from 120 to 700 °C.
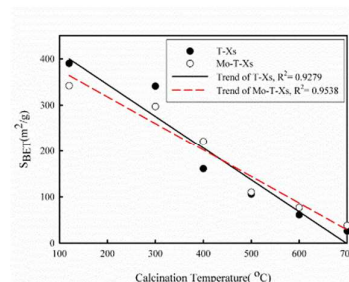
Fig. 2 Correlation between the specific surface area and the calcination temperature of TNTs and Mo-doped TNTs calcined from 120 to 700 °C.

The nano-tubular structure was converted to nano-rods which were ready to crumble into particle shapes at higher temperatures. The tubular-shaped nano-materials obviously disappeared at calcination temperature of 600 °C, and completely collapsed into powder form with particle sizes of 20–40 nm. When calcination temperature increased to 700°C, TiO$_2$ particles sintered into larger nanoparticles of 60–120 nm in size (**Fig. 3E**). The larger particle size of Mo-T-700 made its specific surface area became smaller than that of P25 (**Fig. 3F**) as their values can be seen in **Table 1**.
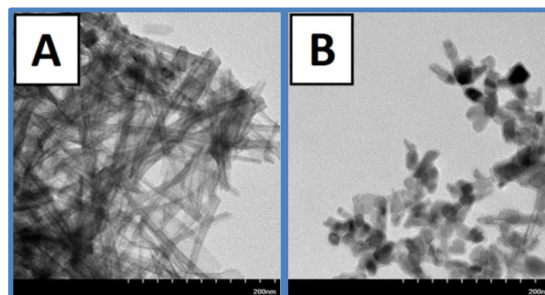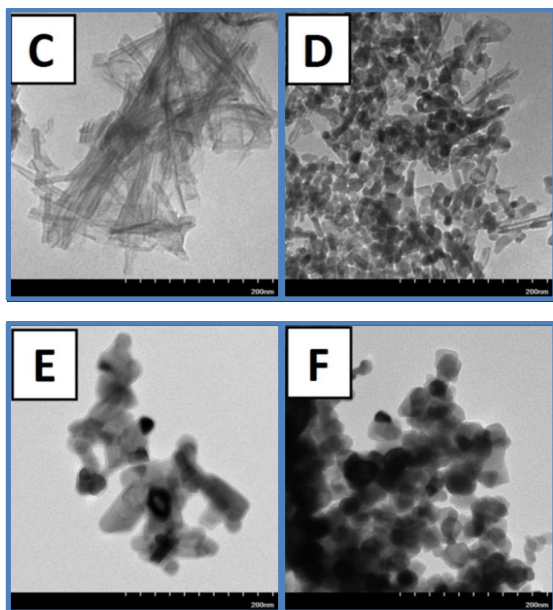
Fig. 3 The TEM images of TNTs and Mo-doped TNTs at different calcination temperatures, (A) T-120; (B) T-500; (C) Mo-T-120; (D) Mo-T-500; (E) Mo-T-700; (F) P25.

These results indicate that the calcination temperature influenced the morphology of Mo-doped TNTs and the phenomenon of shape transformation was similar to those reported in the literature[30,47].

The XRD patterns for Mo-doped TNTs are plotted in **Fig. 4**, with those of P25 and MoOx calcined at 500°C were also added for comparison basis. One can observe that the TNTs characteristic peaks[28,59,39] at 10°、24°、29° and 48° were appeared for Mo-TNTs calcined at temperatures below 400°C. These characteristic peaks gradually decreased with the increase of calcination temperature. On the contrary, TiO_2 anatase peaks[39,60] at 25.3°, 37°, 37.8°, 38.6° and 48.2° started to appear at 400°C and gradually increased with the increase of calcination temperature. At 700°C, rutile peaks[37,39] at 27.5°, 36.2°, 39.4°, 41.3° and 44.1° were found as the result of sintering of TiO_2 structure to form bigger crystalline particles. This phenomenon further confirmed on the TEM results that the TNTs tubular structure started to corrupt at the calcination temperature of around 300 to 500°C. On the other hand, the XRD patterns did not reveal any evidence of MoO_X for Mo-doped TNTs calcined from 120 to 700°C. This might be due to that the MoO_X particles on the surface of Mo-doped TNTs only appeared in a minor amount, or most of the Mo content was incorporated into or covered by the TNTs structure.

The Mo and Ti contents of Mo-doped TNTs were detected by the X-ray photoelectron spectroscopy (XPS) analysis for surface atomic amount and ICP-AES analysis for total weight amount. The amounts of Mo and Ti were then converted to Mo/Ti molar ratio as shown in **Table 2**. From the XPS and ICP-AES results, it is known that Na and Mo were presented in the calcined Mo-doped TNTs. This may indicate that the TNTs structure could be $Na_xH_{2-x}Ti_3O_7·H_2O$[61]. The surface Mo and Na contents of Mo-doped TNTs (from XPS results) were increased

with the increase of calcination temperature, but total amounts of Mo and Na (from ICP-AES results) were not significantly affected by the calcination temperature. Hence, according to **Table 2** as well as the TEM images and XRD results it can be inferred that the presence of Na and Mo on the surface of photocatalysts were from structure degradation of Mo-doped TNTs. In addition, most of the Mo metal species in the Mo-TNTs are possibly incorporated into or covered by the TNTs structure.
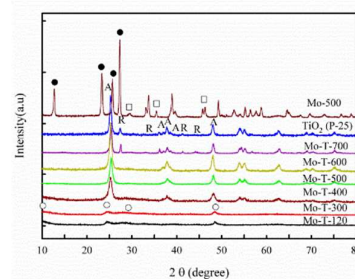
Fig. 4 XRD results of MoOx-500, P-25 and calcined Mo-doped TNTs: (**A**) anatase peaks, (**R**) rutile peaks, (□) MoO_2 peaks, (●) MoO_3 peaks and (○) characteristic peaks of TNT.

Table 2. Atomic concentration[a] and metals contents[b] of Mo-doped TNTs

Catalysts	XPS analysis [a]		ICP-AES analysis [b]	
	Na/Ti (at. %)	Mo/Ti (at.%)	Na/Ti (mol. %)	Mo/Ti (mol. %)
Mo-T-120	4.9	1.8	8.1	1.3
Mo-T-300	29.6	1.5	8.1	1.3
Mo-T-400	49.4	1.9	8.1	1.3
Mo-T-500	49.7	3.0	8.0	1.3
Mo-T-600	67.2	3.5	7.7	1.2
Mo-T-700	61.5	7.4	7.5	1.2

NOTE: [a]The atmoic concentration on the surface of Mo-T-X was detected by XPS analysis. [b]The metal contents of the bulk materials were detected by ICP-AES analysis.

To explore the chemical state of the metal species, the Mo-doped TNTs samples were subjected to XPS analysis and the results are shown in **Fig. 5**. The Na_{1s} and $Mo_{3d3/2}$ peaks were observed from calcined Mo-doped TNTs, this may indicate that the TNTs structure could be $Na_xH_{2-x}Ti_3O_7·H_2O$[61]. The intensity of Na^+ peak (1072.5 eV)[62,63] was gradually enhanced with increasing the calcination temperature, and their atomic concentration of Na^+ can be seen in **Table 2**. This indicates that Na was possibly accommodated into the Mo-doped TNTs framework before Mo-doped TNTs were calcined. And after calcination at high temperature, the Na atoms migrated from the framework into the surface of photocatalyst.

The $Mo_{3d3/2}$ regions showed two peaks at 231.4 and 232.5 eV corresponding to molybdenum in Mo^{5+} and Mo^{6+} oxidation state[64,65], respectively, as seen from **Fig. 5B** for the Mo-doped TNTs.
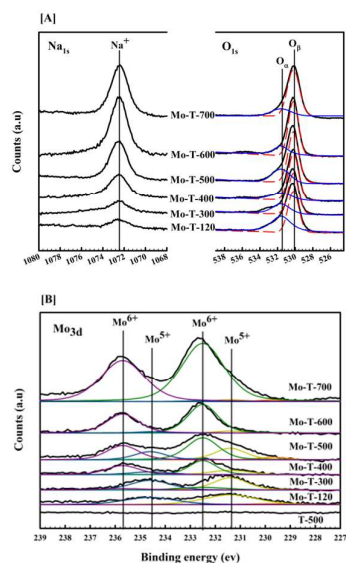
Fig. 5 XPS results of O_{1s}, Na_{1s} and Mo_{3d} for Mo-doped TNTs calcined at different temperature.

It seemed that Mo^{4+} (peaks at 229.7 and 232.9 eV) also appear in Mo-T-500, but with a minor amount. Hence their peaks were not indicated. The Mo^{5+} peak intensity was gradually changed to Mo^{6+} as the calcination temperature was increased. According to TEM and XRD results, it can be inferred that Mo^{5+} was the main form of molybdenum accommodated into the Mo-doped TNTs framework for samples calcined at 300°C and below. Moreover, it did not reveal any evidence of MoO_X for Mo-doped TNTs from XRD patterns. Therefore, the presence of Mo^{5+} was possibly due to the accommodation of Mo into the TNTs framework for materials calcined at low temperature. One can also conclude that the emergence of Na^+ and Mo^{6+} contents due to the increasing temperature was probably from the structure degradation of Mo-doped TNTs.

Furthermore, as seen in **Fig. 5A** the O_{1s} had two peaks, which were O^{2-} and O^- at 529.3–530.2 and 531.3–531.9 eV, respectively. The peak at 529.3–530.2 eV corresponded to the lattice oxygen O^{2-} (hereafter denoted as O_β), and the peak at 531.3–531.9 eV corresponded to the material surface adsorbed oxygen (hereafter denoted as O_α) such as O^{2-} or O^-, which were results of defect oxide or hydroxyl groups[66–68].

The hydroxyl group was due to chemisorbed oxygen on the catalyst surface, while the defect oxide was due to the change of metal species by calcination which could cause a charge imbalance, vacancies and unsaturated chemical bonds on the catalyst surface[68]. One can observe from **Fig. 5A** that the O_α concentration of Mo-doped TNTs was decreased when the calcination temperature increased from 120 to 400 °C, which was due to the dissociation of chemisorbed oxygen on the catalyst's surface. However, the intensity of O_α peak was increased again as the calcination temperature further increased to 500 °C, which was because of the metal species being disaggregated from Mo-doped TNTs structure (such as Mo and Na). The disaggregation of metal species was due to that the tubular structure of Mo-doped TNTs gradually

transformed to particle structure. According to literature[30,69], the structure degradation of TNTs would bring a lot of reduction electrons and lead to metal species reduction. This probably brought some oxygen vacancies and reduced Mo^{6+} to Mo^{5+}. One can also see from **Fig. 5** that only Mo species had obviously changed. Therefore, it can be inferred that oxygen vacancies were arisen from changing of Mo species.

In addition to XPS results, the absorption of visible light could be further used to reveal the state of molybdenum. Dieterle et al.[70] discussed the structural characterization of oxygen defects in MoO_{3-x} and indicated that the absorption bands of energy gap between 0.55 to 3.1 eV could be interpreted as different states of Mo ligand to metal charge transfer (LMCT). Moreover, the intervalence charge transfer (IVCT) band positions at 2.0 eV could be used to determine the sample oxygen stoichiometries of $[Mo^{5+}O_5]$ and $[Mo^{5+}O_6]$ defect centers. Liu et al.[71] further indicated that the presence of oxygen vacancies could possibly enhance the photoreduction efficiency.

Fig. 6 shows the UV–Vis absorption spectra obtained by diffuse reflection of TNTs and Mo-doped TNTs.
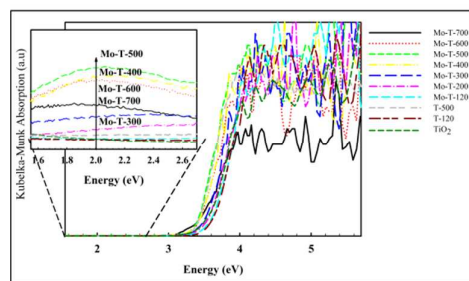
Fig. 6 UV–Vis absorption spectra obtained by diffuse reflections of TNTs and Mo-doped TNTs.
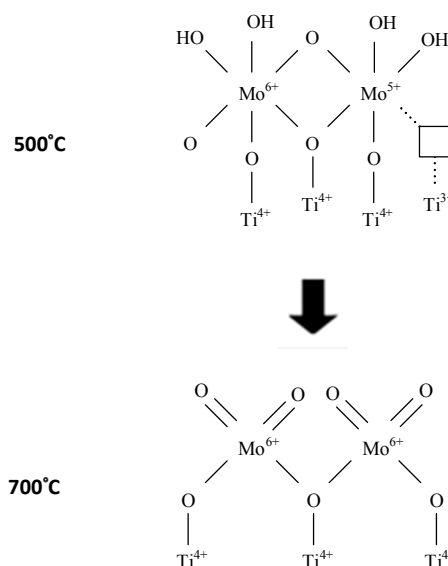
The adsorption band spectra were converted to band energy by the equation of $E_g = 1240/\lambda$ (where λ is wavelength edge of absorption band). It can be observed from **Fig. 6** that Mo-doped TNTs of different calcination temperatures had the absorption edge at lower energy gap (< 2.7 eV). It can also be observed that the absorption capacity at 2.0 eV increased with the increase of calcination temperature in the range of 200 to 500 °C. However, the absorption ability was decreased as Mo-doped TNTs were calcined at temperatures higher than 500 °C. On the other hand, pure TiO_2 (P25), TNTs and Mo-T-120 had no significant absorption edge at lower energy gap (< 2.7 eV, i.e. λ> 460 nm). This may demonstrate that the Mo species in the structure of Mo-T-120 was not effective for visible light adsorption.

Hence, according to analysis results one can infer a possible structure transformation at different calcination temperature ranges for Mo-doped TNTs, as can be seen in **Chart 1**. The possible structure of Mo-T-120 was $[Ti^{4+}$–O–$Mo^{5+}]$. From the XPS result, one can prove that Mo species of Mo-T-120 was in Mo^{5+} oxidation state and O_α was hydroxyl groups. The UV-Vis result can further confirm that the major part of O_α was hydroxyl groups. The Mo-T-120 photocatalyst had a significant

O_α intensity as seen from XPS results, but it did not have significant energy gap at 2.0 eV in UV-Vis results. And the amount of O_α was decreasing when calcination temperature of Mo-TNTs was increased from 120 to 400°C. This is because the Mo species was converted from Mo^{5+} to Mo^{6+} by dehydroxylation on Mo-TNTs surface. Furthermore, the Mo^{6+} was transferred to Mo^{5+} along with the amount of O_α increased when calcination temperature of Mo-TNTs was increased from 300 to 500°C. This is due to structure of titania nanotubes was decomposed to titania anatase by deoxygenation, as can be proved from XRD results. Consequently, this process could produce many electrons to reduce Mo^{6+} to Mo^{5+} oxidation state.

According to the XPS and UV-Vis results, one can observe that the oxygen vacancies of calcined Mo-TNTs were produced between 300 and 700°C, they were probably defected at $[Mo^{5+}–V_{oxygen}–Ti^{3+}]$ and $[Ti^{3+}–V_{oxygen}–Ti^{3+}]$ positions[71]. Then, the Mo^{5+} was transferred to Mo^{6+} once again when calcination temperature was increased over 500°C. This is Mo^{5+} of $[Mo^{5+}–V_{oxygen}–Ti^{3+}]$ oxidized to Mo^{6+} along with the increase of calcination temperature.

The possible reaction pathways are as follows, where V_{oxygen} represents oxygen vacancy.

$$[Ti^{4+}–O–Mo^{5+}] + \tfrac{1}{2} O_2 \rightarrow [Ti^{4+}–O–Mo^{6+}–O^-] \quad (1)$$

$$[Mo^{6+}\overset{H}{\underset{}{–O}}–Ti^{4+}\overset{H}{\underset{}{–O}}—Ti^{4+}] \rightarrow [Mo^{5+}–V_{oxygen}–Ti^{3+}–O–Ti^{4+}] + H_2O \quad (2)$$
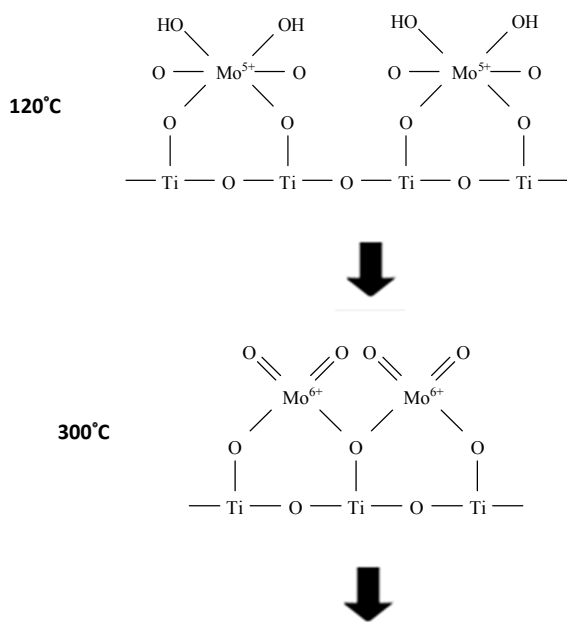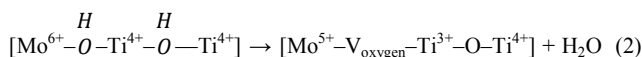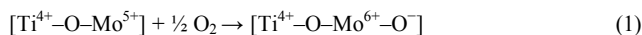
Chart 1 Model of Mo-doped TNTs structure changes reaction pathways at different calcination temperatures.

Photocatalytic reduction of CO_2 and reaction mechanisms

In this study, the photocatalytic reduction of CO_2 using P25 and TNTs were evaluated, and the CH_4 yields are displayed in **Fig. 7**. The CH_4 production yields performed by P25, T-120, and T-500 were similar and almost zero during short term (360 min) test, while relatively higher CH_4 yields were observed for all Mo-doped TNTs. This confirms that the CO_2 reducing ability was provided by adding the Mo metal species into the TNT structure. This result is different from other studies[50,72,73], which usually indicated the Mo-doped TiO_2 could enhance oxidation ability.

It can also be observed from **Fig. 7** that the CH_4 yield increased with the increase of calcination temperature up to 500°C. The CH_4 product yield of Mo-T-500 reached 0.52μmol/g after 360 min, which was the highest among all materials. The CH_4 yield was then decreased as calcination temperature was over 500°C, and the CH_4 production yield of Mo-T-700 was dropped to 0.07μmol/g.

In addition to CH_4 as a desired product of the CO_2 reduction process, CO and TCOCs which can also be used as valuable energy sources were also formed. The yields of CO and TCOCs were measured by FTIR at the end of 360 min experiment and presented in **Fig. 8**, where the CH_4 yield was also added for comparison. The results showed that CO was the major CO_2 reduction product for most of the Mo-doped TNTs. Among all photocatalysts, Mo-T-500 had the highest CO yield of 10.41 μmol/g for, followed by Mo-T-400 (6.33 μmol/g) and Mo-T-600 (6.14 μmol/g). Similar to the trend of CO, TCOCs yield (including CO and CH_4) of Mo-T-500 reached the highest of 13.53 μmol/g, followed by that of Mo-T-400 (8.10 μmol/g) and Mo-T-600 (7.79 μmol/g). In the TCOCs, ethylene and some unknown products were also detected other than CO and CH_4 species, but they were in trace amounts that it had difficulty to

detect them with accuracy due to the detection limit of the instrument.

To ensure that the carbon products of the photocatalytic reduction reaction were not from the MEA solution itself, blank tests were performed with Mo-T-500 as the photocatalyst with UV light on, where only MEA solution was presented as the only carbon source without the introduction of any CO_2. It was observed that there was no CH_4 and CO formation during the blank reaction, while a minor amount of TCOCs other than CH_4 and CO was detected with the yield of 0.16μmol/g. This is only 6.2% of the TCOCs yield (other than
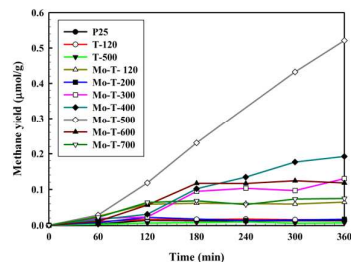

Fig. 7 Methane yields for the photocatalytic reduction of CO_2 in MEA solution using P25, pure TNTs and Mo-doped TNTs.
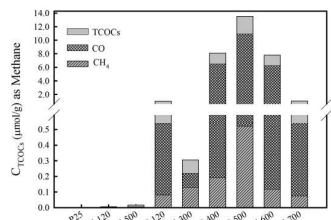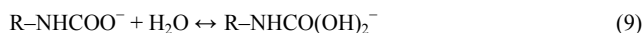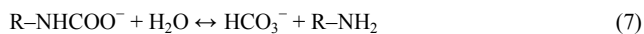

Fig. 8 CH_4 , CO and TCOCs yields for the photocatalytic reduction of CO_2 in MEA solution using P25, pure TNTs and Mo-doped TNTs.
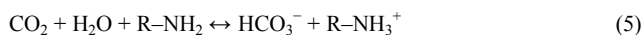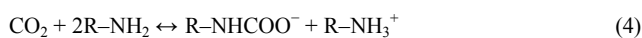
CO and CH_4) as compared to the reaction under the presence of CO_2.

According to the structure transformation at different calcination temperature shown in **Chart 1,** the generation of oxygen vacancies arose between 400 to 600 °C could be the reason for the better product yields of Mo-T-400, Mo-T-500 and Mo-T-600. On the other hand, Mo-T-300 exhibited the poorer yield, which was because that Mo species in the structure of Mo-T-300 was more stable than those in the materials calcined at 400 to 600°C. From these results, it implies that the oxygen vacancies could indeed enhance the photocatalytic activity in the CO_2 reduction reaction. The reaction mechanism of Mo-TNTs for CO_2–MEA absorption reaction is proposed as follows based on the literature[74,75] and our previous study[7],

$$CO_2 + 2R-NH_2 \leftrightarrow R-NHCOO^- + R-NH_3^+ \qquad (4)$$

$$CO_2 + H_2O + R-NH_2 \leftrightarrow HCO_3^- + R-NH_3^+ \qquad (5)$$

$$R-NH_2 + H_2O + CO_2 \leftrightarrow R-NH_3HCO_3 \qquad (6)$$

$$R-NHCOO^- + H_2O \leftrightarrow HCO_3^- + R-NH_2 \qquad (7)$$

$$R-NHCOO^- + R-NH_3^+ \leftrightarrow R-NHCOOH + R-NH_2 \qquad (8)$$
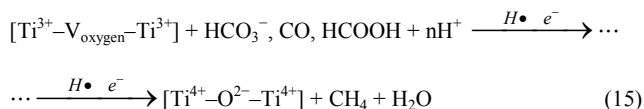
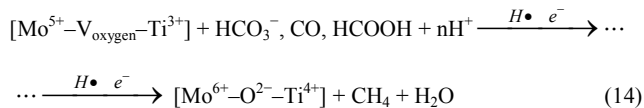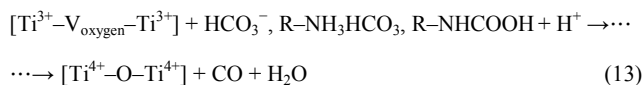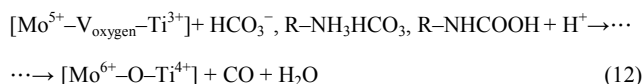$$R-NHCOO^- + H_2O \leftrightarrow R-NHCO(OH)_2^- \qquad (9)$$

The MEA absorption mechanism demonstrates the generation of HCO_3^-, which is a basic carbon source for CO_2 reduction in solution. However, it can be found in the literature[11,75] that HCO_3^- is very difficult to be dissociated from carbon compounds after MEA absorption reaction. Therefore, although MEA has been widely investigated and used as the absorbent in the CO_2 capture process, it has not been considered to be used as absorbent for CO_2 photocatalytic reduction purpose in the literature.

In this study, it is discovered that the oxygen vacancy presented in the Mo-doped photocatalysts was the key factor to induce the CO_2 reduction reaction in the CO_2-MEA solution. Typical reaction of CO_2 reduction revealed in the literature[76,77] was that CO_2^- would be reduced to CO via reaction with H^+, which was due to the dissociation of water, as demonstrated by equations (10) and (11).

$$H_2O + 2h^+ \rightarrow \frac{1}{2}O_2 + 2H^+ \qquad (10)$$

$$CO_2^- + H^+ + e^- \rightarrow CO + OH^- \qquad (11)$$

However, Liu et al.[71] indicated that CO_2^- was directly dissociated by healing the oxygen vacancy sites. This argument was similar to our study results. Therefore, the possible mechanism for photocatalytic CO_2 reduction reaction is proposed in equations (12)-(15) [71,75]. During the CO_2 reduction reaction, CO was possibly formed by direct dissociation of HCO_3^-, $R-NH_3HCO_3$, or $R-NHCOOH$ with the oxygen vacancy sites of [$Mo^{5+}-V_{oxygen}-Ti^{3+}$] and [$Ti^{3+}-V_{oxygen}-Ti^{3+}$]. The produced CO was further reduced to CH_4 via complex reactions with electrons, protons and H^+.

$$[Mo^{5+}-V_{oxygen}-Ti^{3+}] + HCO_3^-, R-NH_3HCO_3, R-NHCOOH + H^+ \rightarrow \cdots$$

$$\cdots \rightarrow [Mo^{6+}-O-Ti^{4+}] + CO + H_2O \qquad (12)$$

$$[Ti^{3+}-V_{oxygen}-Ti^{3+}] + HCO_3^-, R-NH_3HCO_3, R-NHCOOH + H^+ \rightarrow \cdots$$

$$\cdots \rightarrow [Ti^{4+}-O-Ti^{4+}] + CO + H_2O \qquad (13)$$

$$[Mo^{5+}-V_{oxygen}-Ti^{3+}] + HCO_3^-, CO, HCOOH + nH^+ \xrightarrow{H\bullet \quad e^-} \cdots$$

$$\cdots \xrightarrow{H\bullet \quad e^-} [Mo^{6+}-O^{2-}-Ti^{4+}] + CH_4 + H_2O \qquad (14)$$

$$[Ti^{3+}-V_{oxygen}-Ti^{3+}] + HCO_3^-, CO, HCOOH + nH^+ \xrightarrow{H\bullet \quad e^-} \cdots$$

$$\cdots \xrightarrow{H\bullet \quad e^-} [Ti^{4+}-O^{2-}-Ti^{4+}] + CH_4 + H_2O \qquad (15)$$

The photocatalytic reduction efficiencies of photocatalysts were evaluated in terms of the photo-reduction quantum efficiency (PQE) defined by the following equation:[18,22]

$$PQE = \frac{n_e \times \text{Mole of production yield rate}(\mu mol/hr)}{\text{Mole of incident UV photon absorbed rate by catalyst}(\mu mol/hr)} \times 100\%$$

Paper

RSC Advances

Where n_e is the number of moles of electrons required to produce one mole of product from reactant. And the mole of incident UV photons absorbed by photocatalysts was calculated by the following equation:

$$\text{Mole of incident UV photon absorbed by catalyst} = \frac{l_{int}\left(W/cm^2\right) \times A_{proj}\left(cm^2\right)}{hc/\lambda\left(J/\# \, of \; photon\right)}$$

Where l_{int} is the incident light intensity (63 µW/cm^2)

A_{proj} is the area of light irradiation projected in the reactor (278 cm^2)

h is the Plank constant

c is the speed of light

λ is the wavelength of light (365 nm)

From the reaction mechanism in the literature[18], one can assume that 1 mole of methane produced will consume 8 moles of electrons, whereas 1 mole of carbon monoxide produced will only consume 2 moles of electrons.

One of the common approaches to obtain higher values of PQE is to do the experiments at a lower wavelength (e.g. 254nm) as we did in our prior study[53]. And the PQE of 9.18% for CH$_4$ production was obtained using Ti-MCM-41 as the photocatalyst[53]. However, Ti-MCM-41 could not be activated at higher wavelengths for the CO$_2$ photocatalytic reduction.

Table 3. Photo-reduction quantum efficiency (PQE) of catalysts after 360 min UV illumination.

Catalysts	CH$_4$ yield (µmol/g-cat.)	CO yield (µmol/g-cat.)	PQE(%) CH$_4$	CO
TiO$_2$ (P25)	ND	ND	-	-
T-120	ND	ND	-	-
T-500	ND	0.01	-	-
Mo-T-120	0.08	0.46	0.006	0.008
Mo-T-300	0.13	0.09	0.009	0.002
Mo-T-400	0.19	6.33	0.013	0.110
Mo-T-500	0.52	10.41	0.036	0.180
Mo-T-600	0.12	6.14	0.008	0.106
Mo-T-700	0.07	0.47	0.005	0.008

NOTE: "ND" means No Detected.

In this study, it was found that the Mo-doped TNTs could be activated under 365 nm UVA light irradiation. And all CH$_4$ and CO yields of photocatalysts were compared after 360 min of UVA illumination, with the total PQEs summarized in **Table 3**. One can see that the PQEs were 0.005-0.036% and 0.002-0.180%, respectively, for CH$_4$ and CO yields. And the best PQEs for CH$_4$ and CO (0.036% and 0.180%) were achieved when Mo-T-500 was used as the photocatalyst. This seemed to be better than literature data which used the same wavelength of 365 nm for CO$_2$ photocatalytic reduction[78,79], where the values of PQE were in the range of 0.0002–0.0300% for CH$_4$ production.

In addition, the Mo-T-500 was also tested for photocatalytic reduction of CO$_2$ under visible light condition (fluorescent lamp, 840nm, 8W). The product yields for CH$_4$, CO, and TCOCs were 0.15, 0.06, and 0.21µmol/g, respectively, after 360min experiment. And long-term stability test (24hrs) under visible light condition was also performed. It was found that the CH$_4$

yield started to decrease and disappear after 4 hr, while the CO yield continuously increased up to 10.29 µmol/g after 24 hrs. This indicated that there was a re-oxidation of CH$_4$ during the long-term test, which might be due to that the system used in this study was a batch reactor and the product was not continuously taken out to restore back to the fresh condition as the beginning. The low CO$_2$ reduction yields and the stability test under visible light condition indicated that future work is still needed to improve the design of the whole system including light intensity, photocatalyst as well as the reactor design.

Conclusions

The photocatalytic reduction of CO$_2$ using Mo-doped TNTs as photocatalysts with MEA to form CH$_4$ and TCOCs were studied and possible reaction mechanism for Mo-doped TNTs to reduce CO$_2$ in MEA solution was proposed. The results showed that Mo-doped TNTs were good materials for photocatalytic reduction of CO$_2$ with high efficiencies at low-power lamp source. The CH$_4$, CO, and TCOCs production rates by Mo-doped TNTs were much higher than those by P25 and pure TNTs (T-120 and T-500). The photocatalyst of Mo-T-500 had the highest TCOCs yield of 13.53 µmol/g-cat. It also achieved the highest CH$_4$ and CO production rates of 0.52 and 10.41 µmol/g-cat., respectively, and photo-reduction quantum efficiency of 0.036 and 0.180%, respectively, under UVA light. Furthermore, it could be concluded that the structure of molybdenum morphology and oxygen vacancy would affect CO$_2$ photocatalytic reduction efficiency, and the preparation condition of Mo-T-500 had the most oxygen vacancy sites, which was because of the partial disintegration of Mo-T-500 from tubular structure to particle structure that raised more oxygen vacancies. The high CO$_2$ reduction ability discovered in this study will open a new possibility for CO$_2$ utilization by simultaneously capturing and reducing it into valuable energy sources. Future studies should be directed to the development of photocatalysts with higher photo-reduction quantum efficiency under solar light, and to the investigation of reaction mechanisms associated with different test conditions such as light source/intensity, catalyst amount, MEA concentration, and pH value of the test solution.

Acknowledgement

Notes and references

1   J. Hansen, R. Ruedy, M. Sato and K. Lo, *Reviews of Geophysics*, 2010, **48**.
2   Intergovernmental Panel on Climate Change [IPCC] http://www.ipcc.ch/publications_and_data/ar4/wg3/en/ch2s2-5-2.html.

3   M. Balat, H. Balat and C. Öz, *Energy Sources, Part A: Recovery, Utilization, and Environmental Effects*, 2009, **31**, 1473–1486.

4   D. Aaron and C. Tsouris, *Separation Science and Technology*, 2005, **40**, 321–348.

5   L.-Y. Lin and H. Bai, *Chemical Engineering Journal*, 2012, **197**, 215–222.

6   L.-Y. Lin and H. Bai, *Environmental Science & Technology*, 2013, **47**, 4636–4643.

7   A. C. Yeh and H. Bai, *Science of The Total Environment*, 1999, **228**, 121–133.

8   C.-C. Lin, W.-T. Liu and C.-S. Tan, *Industrial & Engineering Chemistry Research*, 2003, **42**, 2381–2386.

9   S. D. Kenarsari, D. Yang, G. Jiang, S. Zhang, J. Wang, A. G. Russell, Q. Wei and M. Fan, *RSC Advances*, 2013, **3**, 22739–22773.

10 Y. Artanto, J. Jansen, P. Pearson, T. Do, A. Cottrell, E. Meuleman and P. Feron, *Fuel*, 2012, **101**, 264–275.

11 G. T. Rochelle, *Science*, 2009, **325**, 1652–1654.

12 K. Teramura, S. Okuoka, H. Tsuneoka, T. Shishido and T. Tanaka, *Applied Catalysis B: Environmental*, 2010, **96**, 565–568.

13 Y. Kohno, H. Hayashi, S. Takenaka, T. Tanaka, T. Funabiki and S. Yoshida, *Journal of Photochemistry and Photobiology A: Chemistry*, 1999, **126**, 117–123.

14 S. Xie, Y. Wang, Q. Zhang, W. Fan, W. Deng and Y. Wang, *Chemical Communications*, 2013, **49**, 2451–2453.

15 M. Anpo, H. Yamashita, K. Ikeue, Y. Fujii, S. G. Zhang, Y. Ichihashi, D. R. Park, Y. Suzuki, K. Koyano and T. Tatsumi, *Catalysis Today*, 1998, **44**, 327–332.

16 S. Kaneco, H. Kurimoto, Y. Shimizu, K. Ohta and T. Mizuno, *Energy*, 1999, **24**, 21–30.

17 B.-J. Liu, T. Torimoto and H. Yoneyama, *Journal of Photochemistry and Photobiology A: Chemistry*, 1998, **115**, 227–230.

18 W.-H. Lee, C.-H. Liao, M.-F. Tsai, C.-W. Huang and J. C. S. Wu, *Applied Catalysis B: Environmental*, 2013, **132–133**, 445–451.

19 M. Zhang, Z. Zhang, Q. Li, X. Wang and J. Yang, *Nanoscale Research Letters*, 2014, **9**, 272.

20 K. Kočí, K. Zatloukalová, L. Obalová, S. Krejčíková, Z. Lacný, L. Čapek, A. Hospodková and O. Šolcová, *Chinese Journal of Catalysis*, 2011, **32**, 812–815.

21 Z. Zhao, J. Fan, M. Xie and Z. Wang, *Journal of Cleaner Production*, 2009, **17**, 1025–1029.

22 I.-H. Tseng, W.-C. Chang and J. C. S. Wu, *Applied Catalysis B: Environmental*, 2002, **37**, 37–48.

23 J. Yu and B. Wang, *Applied Catalysis B: Environmental*, 2010, **94**, 295–302.

24 J.-H. Lee, I.-C. Leu, M.-C. Hsu, Y.-W. Chung and M.-H. Hon, *Journal of Physical Chemistry B*, 2005, **109**, 13056–13059.

25 H. Tsuchiya, J. M. Macak, L. Taveira, E. Balaur, A. Ghicov, K. Sirotna and P. Schmuki, *Electrochemistry Communications*, 2005, **7**, 576–580.

26 Y. Lei, L. D. Zhang, G. W. Meng, G. H. Li, X. Y. Zhang, C. H. Liang, W. Chen and S. X. Wang, *Applied Physics Letters*, 2001, **78**, 1125–1127.

27 K. V. Baiju, S. Shukla, S. Biju, M. L. P. Reddy and K. G. K. Warrier, *Materials Letters*, 2009, **63**, 923–926.

28 A. Nakahira, W. Kato, M. Tamai, T. Isshiki, K. Nishio and H. Aritani, *Journal of Materials Science*, 2004, **39**, 4239–4245.

29 F. Jiang, S. Zheng, L. An and H. Chen, *Applied Surface Science*, 2012, **258**, 7188–7194.

30 B. Vijayan, N. M. Dimitrijevic, T. Rajh and K. Gray, *Journal of Physical Chemistry C*, 2010, **114**, 12994–13002.

31 C.-K. Lee, C.-C. Wang, M.-D. Lyu, L.-C. Juang, S.-S. Liu and S.-H. Hung, *Journal of Colloid and Interface Science*, 2007, **316**, 562–569.

32 R. Doong, C. Tsai and C.-I. Liao, *Separation and Purification Technology*, 2012, **91**, 81–88.

33 J. Fu, S. Cao, J. Yu, J. Low and Y. Lei, *Dalton Transactions*, 2014, **43**, 9158–9165.

34 C. Yu, G. Li, S. Kumar, H. Kawasaki and R. Jin, *Journal of Physical Chemistry Letter*, 2013, **4**, 2847–2852.

35 Y. Wang, J. Yu, W. Xiao and Q. Li, *Journal of Materials Chemistry A*, 2014, **2**, 3847–3855.

36 Y. Liu, H. Yu, H. Lv, S. Zhan, J. Yang, X. Peng, Y. Ren and X. Wu, *Journal of Environmental Sciences*, 2012, **24**, 1867–1875.

37 C. Zhao, L. Liu, Q. Zhang, J. Wang and Y. Li, *Catalysis Science & Technology*, 2012, **2**, 2558–2568.

38 J. Krishna Reddy, G. Suresh, C. H. Hymavathi, V. Durga Kumari and M. Subrahmanyam, *Catalysis Today*, 2009, **141**, 89–93.

39 K. J. A. Raj, M. G. Prakash, R. Mahalakshmy, T. Elangovan and B. Viswanathan, *Catalysis Science & Technology*, 2012, **2**, 1429–1436.

40 Z.-H. Zhao, J.-M. Fan and Z.-Z. Wang, *Journal of Cleaner Production*, 2007, **15**, 1894–1897.

41 W. Zhou, C. Yu, Q. Fan, L. Wei, J. Chen and J. C. Yu, *Chinese Journal of Catalysis*, 2013, **34**, 1250–1255.

42 X. Li, J. Yu, J. Low, Y. Fang, J. Xiao and X. Chen, *Journal of Materials Chemistry A*, 2015, **3**, 2485–2534.

43 X. Li, H. Liu, D. Luo, J. Li, Y. Huang, H. Li, Y. Fang, Y. Xu and L. Zhu, *Chemical Engineering Journal*, 2012, **180**, 151–158.

44 X. Li, J. Wen, J. Low, Y. Fang and J. Yu, *Science China Materials*, 2014, **57**, 70–100.

45 M. Marszewski, S. Cao, J. Yu and M. Jaroniec, *Materials Horizons*, 2015, **2**, 261–278.

46 J. Yu, J. Low, W. Xiao, P. Zhou and M. Jaroniec, *Journal of the American Chemical Society*, 2014, **136**, 8839–8842.

47 R. Doong, S. Chang and C. Tsai, *Applied Catalysis B: Environmental*, 2013, **129**, 48–55.

48 M. Gattrell, N. Gupta and A. Co, *Journal of Electroanalytical Chemistry*, 2006, **594**, 1–19.

49 C. Liu, H. He, P. Zapol and L. A. Curtiss, *Physical Chemistry Chemical Physics*, 2014, **16**, 26584–26599.

50 L. G. Devi and B. N. Murthy, *Catalysis Letters*, 2008, **125**, 320–330.

51 C. Li, D. Zhang, Z. Jiang, Z. Yao and F. Jia, *New Journal of Chemistry*, 2011, **35**, 423–429.

52 L. Gomathi Devi, B. Narasimha Murthy and S. Girish Kumar, *Chemosphere*, 2009, **76**, 1163–1166.

53 H.-Y. Wu, H. Bai and J. C. S. Wu, *Industrial & Engineering Chemistry Research*, 2014, **53**, 11221–11227.

54 N. H. Nguyen and H. Bai, *Journal of Environmental Sciences*, 2014, **26**, 1180–1187.

55 G. Wang, G. Liu, M. Xu, Z. Yang, Z. Liu, Y. Liu, S. Chen and L. Wang, *Applied Surface Science*, 2008, **255**, 2632–2640.

56 V. R. Elías, E. G. Vaschetto, K. Sapag, M. E. Crivello, S. G. Casuscelli and G. A. Eimer, *Topics in Catalysis*, 2011, **54**, 277–286.

57 G. Moretti, A. M. Salvi, M. R. Guascito and F. Langerame, *Surface and Interface Analysis*, 2004, **36**, 1402–1412.

58 T. Horikawa, M. Katoh and T. Tomida, *Microporous and Mesoporous Materials*, 2008, **110**, 397–404.

59 B. D. Yao, Y. F. Chan, X. Y. Zhang, W. F. Zhang, Z. Y. Yang and N. Wang, *Applied Physics Letters*, 2003, **82**, 281–283.

60 G. Tsilomelekis and S. Boghosian, *Catalysis Science & Technology*, 2013, **3**, 1869–1888.

61 T. Gao, H. Fjellvåg, P. Norby, T. Gao, H. Fjellvåg and P. Norby, *Inorganic Chemistry*, 2009, **48**, 1423–1432.

62 H. Tomaszewski, K. Eufinger, H. Poelman, D. Poelman, R. De Gryse, P. F. Smet and G. B. Marin, *International Journal of Photoenergy*, 2006, **2007**, e95213.

63 P.-Y. Brisson, H. Darmstadt, M. Fafard, A. Adnot, G. Servant and G. Soucy, *Carbon*, 2006, **44**, 1438–1447.

RSC Advances Accepted Manuscript

64 Y. Shen, T. Xiong, H. Du, H. Jin, J. Shang and K. Yang, *Journal of Sol-Gel Science and Technology*, 2009, **50**, 98–102.
65 T. He and J. Yao, *Journal of Photochemistry and Photobiology C: Photochemistry Reviews*, 2003, **4**, 125–143.
66 F. Liu, H. He, Y. Ding and C. Zhang, *Applied Catalysis B: Environmental*, 2009, **93**, 194–204.
67 M. Kang, E. D. Park, J. M. Kim and J. E. Yie, *Applied Catalysis A: General*, 2007, **327**, 261–269.
68 Z. Wu, R. Jin, Y. Liu and H. Wang, *Catalysis Communications*, 2008, **9**, 2217–2220.
69 B. K. Vijayan, K. C. Schwartzenberg, J. Wu and K. A. Gray, *Journal of Molecular Catalysis A: Chemical*, 2015, **402**, 23–28.
70 M. Dieterle, G. Weinberg and G. Mestl, *Physical Chemistry Chemical Physics*, 2002, **4**, 812–821.
71 L. Liu, F. Gao, H. Zhao and Y. Li, *Applied Catalysis B: Environmental*, 2013, **134–135**, 349–358.
72 M. S. Jeon, W. S. Yoon, H. Joo, T. K. Lee and H. Lee, *Applied Surface Science*, 2000, **165**, 209–216.
73 K. Y. Song, M. K. Park, Y. T. Kwon, H. W. Lee, W. J. Chung and W. I. Lee, *Chemistry of Materials,* 2001, **13**, 2349–2355.
74 M. Hasib-ur-Rahman and F. Larachi, *Industrial & Engineering Chemistry Research*, 2013, **52**, 17682–17685.
75 Y. Matsuzaki, H. Yamada, F. A. Chowdhury, T. Higashii and M. Onoda, *Journal of Physical Chemistry A*, 2013, **117**, 9274–9281.
76 T. Inoue, A. Fujishima, S. Konishi and K. Honda, *Nature*, 1979, **277**, 637–638.
77 K. Kočí, L. Obalová and Z. Lacný, *Chemical Papers*, 2008, **62**, 1–9.
78 S. Murcia-López, V. Vaiano, M. C. Hidalgo, J. A. Navío and D. Sannino, *Photochemical & Photobiological Sciences*, 2015, **14**, 678–685.
79 J. C. S. Wu, T.-H. Wu, T. Chu, H. Huang and D. Tsai, *Topics in Catalysis*, 2008, **47**, 131–136.